Monthly Notices of the ROYAL ASTRONOMICAL SOCIETY

MNRAS **536,** 714–727 (2025) https://doi.org/10.1093/mnras/stae2610
Advance Access publication 2024 November 21

ExoMol line lists – LXIV. Empirical rovibronic spectra of phosphorous mononitride (PN) covering the IR and UV regions

Mikhail Semenov [1], Nayla El-Kork,[2] Sergei N. Yurchenko [1] and Jonathan Tennyson [1]★

[1]*Department of Physics and Astronomy, University College London, Gower Street, WC1E 6BT London, UK*
[2]*Space and Planetary Science Center, Khalifa University, Abu-Dhabi, UAE*

Accepted 2024 November 19. Received 2024 November 15; in original form 2024 April 24

ABSTRACT

A new phosphorous mononitride ($^{31}P^{14}N$ and $^{31}P^{15}N$) line list PaiN covering infrared, visible, and ultraviolet regions is presented. The PaiN line list extending to the $A\,^1\Pi$–$X\,^1\Sigma^+$ vibronic band system replaces the previous YYLT ExoMol line list for PN. A thorough analysis of high-resolution experimental spectra from the literature involving the $X\,^1\Sigma^+$ and $A\,^1\Pi$ states is conducted, and many perturbations to the $A\,^1\Pi$ energies are considered as part of a comprehensive MARVEL (Measured-Active-Rotational-Vibrational-Energy-Levels) study. Ab initio potential energy and coupling curves from the previous work are refined by fitting their analytical representations to 1224 empirical energy levels determined using the MARVEL procedure. The PaiN line list is compared to previously observed spectra, recorded and calculated lifetimes, and previously calculated partition functions. The ab initio transition dipole moment curve for the A–X band is scaled to match experimentally measured lifetimes. The line list is suitable for temperatures up to 5000 K and wavelengths longer than 121 nm. PaiN is available from www.exomol.com.

Key words: molecular data – astronomical data bases: miscellaneous – exoplanets – stars: carbon.

1 INTRODUCTION

Phosphorus mononitride (PN) has emerged as a molecule of significant astrophysical interest, challenging earlier theoretical predictions about the abundance of phosphorus-bearing species in space. While phosphorus monoxide (PO) was initially expected to be the most prevalent diatomic phosphorus molecule based on early laboratory experiments (Thorne et al. 1984; Millar, Bennett & Herbst 1987), there has been a significant statistical increase of PN detections in comparison to PO across various astronomical environments (Fontani 2024), although often with lower abundances compared to PO when both were present (Lefloch et al. 2016; Fontani et al. 2019). PN has been detected in star-forming regions like the Orion Nebula (Turner & Bally 1987; Yamaguchi et al. 2011), in the circumstellar envelopes of evolved stars such as asymptotic giant branch stars, and red supergiants such as VY Canis Majoris (Ziurys et al. 2007; Milam et al. 2008; Ziurys, Schmidt & Bernal 2018), as well as in cold molecular clouds with temperatures ranging from 10 to 100 K (Rivilla et al. 2018). Recent astrophysical developments include the first extragalactic detection of PN by Haasler et al. (2022) and its detection at the edge of our Galaxy (Koelemay, Gold & Ziurys 2023), further reinforcing the importance of PN as an astrophysical species. This unexpected observational prominence of PN over PO highlights gaps in our understanding of interstellar phosphorus chemistry and may be attributed to differences in their excitation conditions or detection sensitivities. This underscores the need for accurate spectroscopic data to facilitate the detection and analysis of phosphorus-bearing molecules.

The full summary of experimental works conducted has been thoroughly described previously (Millar et al. 1987; Tobola et al. 2007; Milam et al. 2008; De Beck et al. 2013; Yorke et al. 2014; Fontani et al. 2016; Fontani et al. 2019; Qin, Zhao & Liu 2019; Semenov et al. 2021; Haasler et al. 2022; Gomes et al. 2023; Fontani 2024).

A recent extended ab initio study was recently conducted by Liu et al. (2022), reporting 39 electronic states with spin–orbit couplings. This ab initio study further confirmed the difficulty of modelling the $A\,^1\Pi$ state due to the multiple interactions with adjacent electronic states involving almost all vibrational levels. Tian et al. (2024) more recently reported a variationally improved Hulburt–Hirschfelder potential model for the PN ground state, using it to predict different thermodynamic properties such as the molar heat capacity, entropy, enthalpy, and Gibbs free energy.

Another recent study by Eckhardt et al. (2022) came up with a different methodology for producing PN, which should make future spectroscopic studies on the molecule easier. A study in photochemistry by Zhu et al. (2024) suggested additional pathways for PN creation in the interstellar medium and star-forming regions compared to the earlier studies by Tofan & Velian (2020), Rivilla et al. (2020), and Sil et al. (2021).

Previously, an ExoMol line list for PN (YYLT) covering rovibrational transitions within its $X\,^1\Sigma^+$ ground state was reported by Yorke et al. (2014). The YYLT line list was generated using an empirically refined potential energy curve (PEC) and an ab initio dipole moment curve (DMC) of PN. The present study replaces the YYLT line list by both improving the treatment of the $X\,^1\Sigma^+$ state and extending it to include the $A\,^1\Pi$ state using the standard ExoMol methodology (Tennyson et al. 2024b). The ultraviolet (UV) absorption cross-sections of molecules are important

★ E-mail: j.tennyson@ucl.ac.uk

not only for direct observations in the UV but also for utilization in atmospheric chemistry calculations (Chubb et al. 2024). The UV molecular data on PN will be relevant to the *Hubble Space Telescope* (*HST*; WFC3/UVIS instrument covering 200–1000 μm), the *Galaxy Evolution Explorer* (*GALEX*; 135–280 nm), and the Habitable Worlds Observatory (HWO) future mission concept.

In this study, we present a systematic analysis of all experimental high-resolution transition data and derive empirical energy levels for $^{31}P^{14}N$. These empirical energy levels are determined using the MARVEL (Measured-Active-Rotational-Vibrational-Energy-Levels) procedure (Furtenbacher, Császár & Tennyson 2007; Tóbiás et al. 2019) by inverting all $^{31}P^{14}N$ experimental frequencies obtained from the literature (Curry, Herzberg & Herzberg 1933; Hoeft, Tiemann & Törring 1972; Wyse, Gordy & Manson 1972; Coquart & Prudhomme 1981; Ghosh, Verma & VanderLinde 1981; Maki & Lovas 1981; Verma, Ghosh & Iqbal 1987; Ahmad & Hamilton 1995; Le Floch et al. 1996; Cazzoli, Cludi & Puzzarini 2006) to produce a self-consistent set of experimentally derived energies for this molecule. We provide a unified account of all the experimentally suggested perturbations in $A\,^1\Pi$ (Ghosh et al. 1981; Le Floch et al. 1996), primarily caused by the $C\,^1\Sigma^-$, $D\,^1\Delta$, $b\,^3\Pi$, $d\,^3\Delta$, and $e\,^3\Sigma^-$ electronic states. The $A\,^1\Pi$–$X\,^1\Sigma^+$ transition dipole moment is scaled to replicate the lifetimes measured by Moeller, McKeever & Silvers (1975). We refine the $A\,^1\Pi$ and $X\,^1\Sigma^+$ PECs and coupling curves representing the $A\,^1\Pi$–$X\,^1\Sigma^+$ system starting from our previous ab initio models (Semenov et al. 2021; Ushakov et al. 2023) and using the empirical (MARVEL) energies of $^{31}P^{14}N$ to produce a semi-empirical line list PaiN for $^{31}P^{14}N$ and its isotopologue $^{31}P^{15}N$ valid over an extended temperature range.

2 MARVEL

The MARVEL algorithm (Furtenbacher et al. 2007; Furtenbacher & Császár 2012a; Tóbiás et al. 2019; Tennyson et al. 2024a) constructs a self-consistent set of rovibronic energies derived from experimental transition data. By using the experimental uncertainties for the initial weights in a weighted linear least-squares protocol, MARVEL forms associated energy levels and their respective uncertainty. Through multiple iterations in which the original weights are adjusted, MARVEL then forms a self-consistent set of energies by adjusting the uncertainty for each transition until they agree with the wider spectroscopic network (SN; Furtenbacher & Császár 2012b). This also allows one to remove the so-called bad lines – transitions that are not in agreement with the rest of the SN. Here, we use the MARVEL 4 algorithm of Tennyson et al. (2024a).

For $^{31}P^{14}N$, all available and identifiable experimental transitions have been collected from the literature and processed using the MARVEL procedure. The transition frequencies of $^{31}P^{14}N$ extracted in this paper cover two main bands of PN involving the $X\,^1\Sigma^+$ and $A\,^1\Pi$ electronic states, $X\,^1\Sigma^+$–$X\,^1\Sigma^+$, $A\,^1\Pi$–$X\,^1\Sigma^+$, as summarized in Table 1. The transition data from the $E\,^1\Sigma^+$–$X\,^1\Sigma^+$ system is outside the current model, and thus, it has not been used in the MARVEL analysis. The empirical (MARVEL) energy levels of the $X\,^1\Sigma^+$ and $A\,^1\Pi$ states of $^{31}P^{14}N$ derived are depicted in Fig. 1.

2.1 Experimental sources of $^{31}P^{14}N$

All the available sources of experimental transitions of $^{31}P^{14}N$ considered in this work are reviewed below (see also Table 1).

33CuHeHe (Curry et al. 1933) is the first detection of PN in laboratory setting. In their work, they reported 570 transitions of the $A\,^1\Pi$–$X\,^1\Sigma^+$ system for the vibrational bands (0, 0), (0, 1), (0, 2), (1, 0), (1, 2), and (1, 3).

72HoTiTo (Hoeft et al. 1972) reported five $X\,^1\Sigma^+$ state hyperfine transitions $J = 1 - 0$ within the $v = 1$ and 0 vibrational states, which we deperturbed to two rotational transition frequencies for the MARVEL analysis using the methodology outlined by Bowesman et al. (2022).

72WyGoMa (Wyse et al. 1972) recorded 19 $X\,^1\Sigma^+$ state rotational transitions within the $v = 0, 1, 2, 3$ and 4 vibrational states using microwave spectroscopy.

81GhVeVa (Ghosh et al. 1981) reported 1680 rovibronic transitions of the $A\,^1\Pi$–$X\,^1\Sigma^+$ system arising from 33 (v', v'') bands with v' ranging from 0 to 9 and v'' ranging from 0 to 10.

81MaLo (Maki & Lovas 1981) reported 22 $X\,^1\Sigma^+$ state rovibrational transitions system in the (1, 0), (2, 1), (3, 2), and (4, 3) bands.

81CoPr (Coquart & Prudhomme 1981) reported 1382 rovibronic transitions of the $E\,^1\Sigma^+$–$X\,^1\Sigma^+$ band originally with unidentified upper vibrational levels labelled simply as $v, v + 1, v + 2$, etc. Using the results produced by Verma & Ghosh (1984), we were able to determine their reference value v to be $v = 4$ and assign all the other vibrational levels accordingly. However, due to the low quality of data from Coquart & Prudhomme (1981) compared to other sources (i.e. higher uncertainty), the presence of unidentified transitions to perturbing dark states, and often conflicting assignments, we found that these issues negatively impacted the reconstruction of the $X\,^1\Sigma^+$ state energies. We, therefore, decided to exclude this data from the MARVEL analysis, but keep it in the MARVEL transition file by setting the transition frequencies negative as per the MARVEL procedure.

87VeGhIq (Verma et al. 1987) reported 961 rovibronic transition with unidentified bands of $^{31}P^{14}N$ $\alpha\,^1\Pi$–$X\,^1\Sigma^+$, $\beta\,^1\Pi$–$X\,^1\Sigma^+$, $\delta\,^1\Sigma^+$–$X\,^1\Sigma^+$, and $\gamma\,^1\Sigma^+$–$X\,^1\Sigma^+$. However, because both the vibrational bands and electronic upper state assignment were undefined, this experimental data set was omitted from the MARVEL procedure at this stage but is provided as a supplementary in the MARVEL format.

95AhHa (Ahmad & Hamilton 1995) reported 62 $X\,^1\Sigma^+$ rovibrational transitions in the (1, 0) fundamental band obtained using an FTIR (Fourier Transform Infrared) spectrometer.

96LeMeD (Le Floch et al. 1996) reported 1680 rovibronic transitions of the $A\,^1\Pi$–$X\,^1\Sigma^+$ band system in the (0, 0), (0, 1), (0, 2), (1, 0), (1, 2), (1, 3), (2, 1), (2, 0), (2, 3), (2, 4), (3, 2), and (3, 1) bands.

06CaClPu (Cazzoli et al. 2006): reported 13 $X\,^1\Sigma^+$ state transitions, including 12 hyperfine-resolved ones, which we deperturbed to 3 rotational transitions in the $v = 0$ state for MARVEL analysis using the methodology outlined of Bowesman et al. (2022).

2.2 $A\,^1\Pi$ perturbations

As can be seen in previous ab initio works by Abbiche et al. (2014), Qin et al. (2019), and Liu et al. (2022), the $A\,^1\Pi$ state is surrounded by multiple electronic states within which it interacts with, including $D\,^1\Delta$, $e\,^3\Sigma^-$, and $d\,^3\Delta$ (see Fig. 3). The spin–orbit couplings with these dark states are of the order of 20–30 cm^{-1} (see Semenov et al. 2021).

The experimental evidence given by Ghosh et al. (1981) and Le Floch et al. (1996) points to multiple crossings for $v = 0, 1, 2, 3$, and 7. It has also been suggested that $A\,^1\Pi$ is perturbed by the $E\,^1\Sigma^+$ state at $v = 14$ by Liu et al. (2022), but there is no other experimental

Table 1. Breakdown of the assigned transitions by electronic bands for the sources used in this MARVEL study. *A* and *V* are the numbers of the available and validated transitions, respectively. The minimum, maximum, and mean uncertainties (Unc.) obtained using the MARVEL 4.0 procedure are given in cm^{-1}.

Electronic band	Vibrational bands	*J* Range	Range (cm^{-1})	*A*/*V*	Min Unc. $(cm)^{-1}$	Max Unc. $(cm)^{-1}$	Mean Unc. $(cm)^{-1}$
33CuHeHe							
$A\,^1\Pi$–$X\,^1\Sigma^+$	(0, 0), (0, 1), (0, 2), (1, 0), (1, 2), (1, 3)	7–65	36681.4–40758.0	570/199	0.20	0.48	0.21
72HoTiTo							
$X\,^1\Sigma^+$–$X\,^1\Sigma^+$	(0, 0), (1, 0)	0–1	1.556319159–1.567427720	2/2	4.59×10^{-9}	2.88×10^{-8}	1.78×10^{-8}
72WyMaGo							
$X\,^1\Sigma^+$–$X\,^1\Sigma^+$	(0, 0), (1, 1), (2, 2), (3, 3), (4, 4)	2–8	3.112628–12.537217	19/19	6.67×10^{-6}	6.67×10^{-6}	6.67×10^{-6}
81MaLo							
$X\,^1\Sigma^+$–$X\,^1\Sigma^+$	(1, 0), (2, 1), (3, 2), (4, 3)	2–52	1217.216–1318.591	22/22	3.00×10^{-4}	3.10×10^{-3}	1.38×10^{-3}
81CoPr							
$E\,^1\Sigma^+$–$X\,^1\Sigma^+$	(4, 3), (5, 2), (6, 1), (6, 2), (6, 5), (7, 1), (8, 0), (8, 1), (8, 4), (9, 0), (9, 3), (10, 0), (10, 2), (11, 0)	0–62	52355.10–61787.57	1382/0	5.00×10^{-2}	5.00×10^{-2}	5.00×10^{-2}
81GhVeVa							
$A\,^1\Pi$–$X\,^1\Sigma^+$	(0, 0), (0, 1), (0, 2), (1, 0), (1, 2), (1,3), (1, 4), (2, 0), (2, 3), (2, 4), (2, 5), (3, 1), (3, 2), (3, 3), (3, 4), (3, 5), (3,6), (4, 1), (4, 2), (4, 5), (4, 6), (4, 7), (4, 8), (5,2), (5, 7), (5, 8), (5, 9), (6, 3), (6, 9), (6, 10), (7, 3), (7, 10), (9, 5)	0–39	33334.96–43081.72	2188/1586	5.00×10^{-2}	2.76×10^{-1}	5.18×10^{-2}
95AhHa							
$X\,^1\Sigma^+$–$X\,^1\Sigma^+$	(1, 0)	0–33	1273.296–1368.494	62/61	2.00×10^{-3}	2.00×10^{-3}	2.00×10^{-3}
96LeMeDu							
$A\,^1\Pi$–$X\,^1\Sigma^+$	(0, 0), (0, 1), (0, 2), (1, 0), (1, 2), (1, 3), (2, 1), (2, 0), (2, 3), (2, 4), (3, 2), (3, 1)	1–69	36459.57–41856.93	1680/959	5.00×10^{-2}	3.12×10^{-1}	5.14×10^{-2}
06CaClPu							
$X\,^1\Sigma^+$–$X\,^1\Sigma^+$	(0, 0), (1, 1), (2, 2), (3, 3), (4, 4), (1, 0), (2, 1), (3, 2), (4, 3)	0–52	1.5674270–10.9705230	16/16	2.00×10^{-7}	1.33×10^{-6}	9.70×10^{-7}

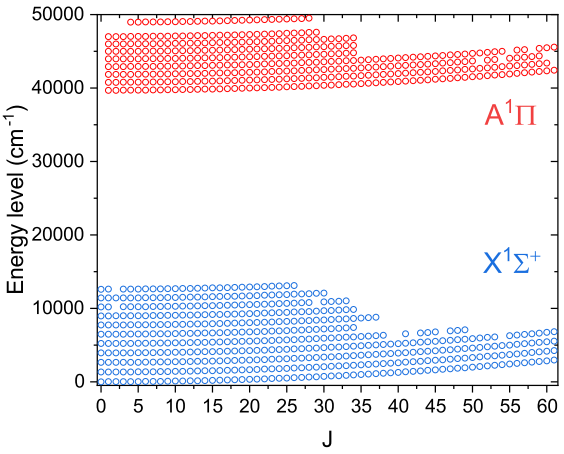

Figure 1. Empirical energy levels derived from experimental transitions using MARVEL.

evidence in the required region to confirm this. Below, we provide a detailed description of the state crossings and resulting perturbations for each known vibrational state of $A\,^1\Pi$ affected.

The $A\,^1\Pi v = 0$ state is believed to be perturbed by $D\,^1\Delta$, $e\,^3\Sigma^-$ (Le Floch et al. 1996), and $d\,^3\Delta$ (Ghosh et al. 1981). There is general agreement on the crossing at $J = 16$, but Le Floch et al. (1996) could not verify the suggested crossing by Ghosh et al. (1981) at $J = 9$ by $d\,^3\Delta$ and the work of Ghosh et al. (1981) also does not extend to $J = 61$ to confirm the $e\,^3\Sigma^-$ crossing suggested by Le Floch et al. (1996). Both the $J = 9$ and $J = 16$ suspected crossings are confirmed within our MARVEL data by means of the rotational decomposition of energy levels, as can be seen in Fig. 2.

The $A\,^1\Pi v = 1$ state is perturbed by the $e\,^3\Sigma^-$ state at $J = 46$ and 53 as predicted by Ghosh et al. (1981) and at $J = 46$, 53, and 61 suggested by Le Floch et al. (1996). These perturbations are confirmed in the rotational decomposition of our reduced MARVEL energies for $v = 1$ shown in Fig. 2.

The $A\,^1\Pi v = 2$ state is heavily perturbed by the $e\,^3\Sigma^-$ state at $J = 28$, 35 and 40 as predicted by both Ghosh et al. (1981) and Le

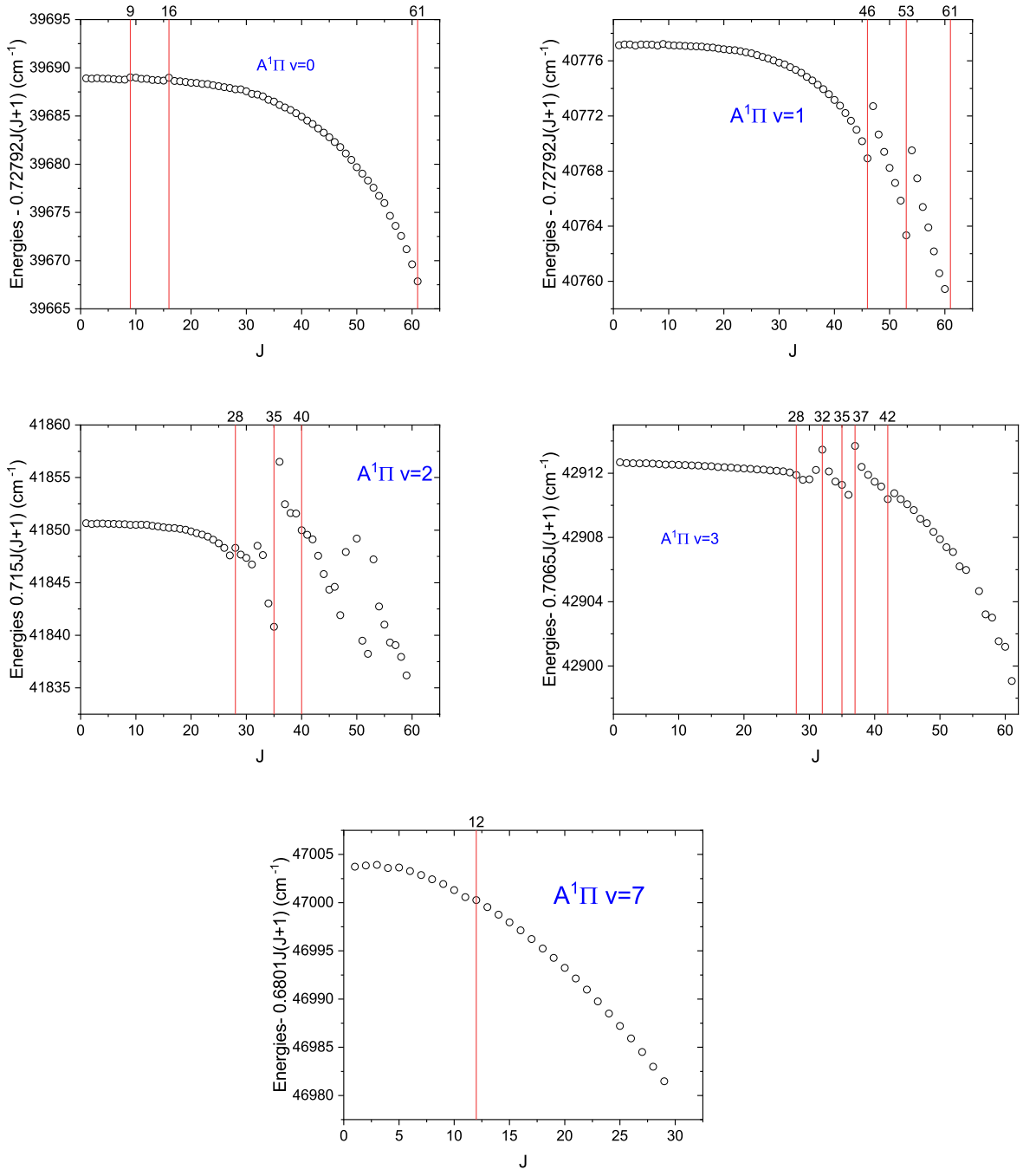

Figure 2. Reduced empirical energy term values for the $v = 0, 1, 2, 3, 7$ of the $A\,^1\Pi$ state of PN in the rotational decomposition. The rotational B constants used for each v were taken from Ghosh et al. (1981). The lines indicate J values corresponding to state crossings as suggested by Ghosh et al. (1981) and Le Floch et al. (1996).

Floch et al. (1996); however, the impact of the crossing with the $e\,^3\Sigma^-$ state is much more profound than in the $v = 1$ state. The crossing points are confirmed by us and shown in Fig. 2.

The $A\,^1\Pi v = 3$ state is believed to be perturbed by $b\,^3\Pi$ or $D\,^1\Delta$ at $J = 28$ according to Ghosh et al. (1981), whereas Le Floch et al. (1996) believe that $d\,^3\Delta$ and $C\,^1\Sigma^-$ are the main perturbing electronic states at $J = 32$, 37, 35, and 42. Our MARVEL data agree on the crossings suggested by Le Floch et al. (1996), even though it is hard to distinguish separate perturbations at $J = 35$ and $J = 37$. Our MARVEL $v = 3$ energy is perturbed at $J = 28$, it is hard to verify if the crossing is by $b\,^3\Pi$ or $D\,^1\Delta$ as suggested by Ghosh et al. (1981). All the suggested crossings are illustrated in the reduced energy diagram in Fig. 2.

Both Ghosh et al. (1981) and Le Floch et al. (1996) suggest that the $A\,^1\Pi v = 7$ state is crossed by the $D\,^1\Delta$ at $J = 11$. The resulting perturbation is much weaker than for the lower lying $A\,^1\Pi v$ states but can still be seen in Fig. 2.

The multiple crossings involving the $A\,^1\Pi$ state, which are summarized in Table 2, make it hard to model the spectra. An advantage of the MARVEL approach is that it does not depend on a

Table 2. Summary of positions of the crossings J_c of the vibronic states v, $A\,^1\Pi$ caused by perturbations by other electronic states as suggested by different experimental studies.

$A\,^1\Pi$ v	J_c	Suggested perturbing state(s)	Source
0	8/9	$d\,^3\Delta$	81GhVeVa
0	15/16	$D\,^1\Delta$	96LeMeDu
0	16/17	$d\,^3\Delta$	81GhVeVa
0	61/62	$e\,^3\Sigma^-$	96LeMeDu
1	45/46	$e\,^3\Sigma^-$	81GhVeVa
1	46/47	$e\,^3\Sigma^-$	96LeMeDu
1	52/53	$e\,^3\Sigma^-$	81GhVeVa
1	53/54	$e\,^3\Sigma^-$	96LeMeDu
1	60/61	$e\,^3\Sigma^-$	96LeMeDu
2	27/28	$e\,^3\Sigma^-$	96LeMeDu
2	27/28	$e\,^3\Sigma^-$	81GhVeVa
2	35/36	$e\,^3\Sigma^-$	96LeMeDu
2	35/36	$e\,^3\Sigma^-$	81GhVeVa
2	40/41	$e\,^3\Sigma^-$	96LeMeDu
3	28/29	$b\,^3\Pi$ $D\,^1\Delta$	81GhVeVa
3	31/32	$d\,^3\Delta$	96LeMeDu
3	36/37	$d\,^3\Delta$	96LeMeDu
3	34/35	$C\,^1\Sigma^-$	96LeMeDu
3	42/43	$d\,^3\Delta$	96LeMeDu
7	11/12	$D\,^1\Delta$	96LeMeDu, 81GhVeVa

model and is, therefore, able to capture the energies of the perturbed levels correctly; something that is very hard to do with effective Hamiltonians (EHs). Our spectroscopic model also struggles to reproduce the many perturbations, as there is little information on the perturbing states. However, observed transitions involving perturbed levels with $J > 30$ for $v = 1$, 2 and 3 did not always yield a consistent SN, which led us to exclude multiple transitions with higher J, as can be seen in Fig. 1. Ideally, we would be able to assign the affected transitions to the dark states, stealing intensity from the $A\,^1\Pi$ state, and fully model the interactions; however, because of the ambiguous experimental assignment of vibrational levels of the interacting dark states, we elected not to include these in our MARVEL SN. This results in sacrificing the quality of the calculated energies around the crossings within our spectroscopic model, but also providing a better fit overall to the remaining energies.

3 SPECTROSCOPIC MODEL AND REFINEMENT

For our spectroscopic model and its subsequent refinement, we use the variational diatomic nuclear-motion code DUO[1] (Yurchenko et al. 2016) to solve the coupled system of Schrödinger equations for the $X\,^1\Sigma^+$ and $A\,^1\Pi$ systems of PN. In these calculations, we used the Sinc DVR method for the vibrational degree of freedom on a grid of 701 points ranging from 1.0 to 5.0 Å.

Our spectroscopic model selection for the description of the $A\,^1\Pi$ – $X\,^1\Sigma^+$ system is fully uncoupled from the other electronic states of PN. The corresponding PECs and couplings are shown in Figs 3 and 4. In Fig. 3, we also show ab initio curves corresponding to other electronic states from this region from our previous work (Semenov et al. 2021), not considered in the current model: $a\,^3\Sigma^+$, $b\,^3\Pi$, $d\,^3\Delta$, $e\,^3\Sigma^-$, $C\,^1\Sigma^-$, $D\,^1\Delta$, and $E\,^1\Sigma^+$. Except for $C\,^1\Sigma^-$ and $E\,^1\Sigma^+$, these are all 'dark' states with respect to the transitions from/to the ground electronic state $X\,^1\Sigma^+$. Indeed, $a\,^3\Sigma^+$, $e\,^3\Sigma^-$, $b\,^3\Pi$, and $d\,^3\Delta$ have different multiplicities and are therefore dipole forbidden (before the coupling), while the $D\,^1\Delta$ state is also dipole forbidden due to the selection rule

$$\Delta\Lambda = 0, \pm 1.$$

Here, Λ is the projection of the electronic angular momentum on the molecular axis and $\Lambda = 0, \pm 1, \pm 2$ for Σ, Π, and Δ, respectively. Although the $C\,^1\Sigma^-$ and $E\,^1\Sigma^+$ states are not dipole forbidden for $X\,^1\Sigma^+$, they were deemed to be unimportant for the $A\,^1\Pi$–$X\,^1\Sigma^+$ system and hence also excluded. The $C\,^1\Sigma^-$–$X\,^1\Sigma^+$ band is weak because of the small Franck–Condon factor (see also Semenov et al. 2021), while the $E\,^1\Sigma^+$–$X\,^1\Sigma^+$ band is higher by about 20 000 cm^{-1}. The main reasons for not including these states are (i) insufficient quality of the ab initio data, (ii) a large number of local perturbations within the $A\,^1\Pi$ region (see Section 2.2) and (iii) a severe lack of the experimental data required for proper description of the underlying PECs and other couplings. Therefore, in this work, for the spectroscopic description of the $A\,^1\Pi$–$X\,^1\Sigma^+$ system, we opted for a complete exclusion of these interactions instead of having them all in the wrong places. However, one should be aware that the exclusion of these interactions means that intensity borrowing and shifts in spectral lines within this perturbed region may occur, potentially exceeding the stated line uncertainties. Such effects are not expected to significantly influence predictions when the line lists are used for atmospheric chemistry modelling.

3.1 PECs

As a starting point for this model, the results from the two previous studies (Semenov et al. 2021; Ushakov et al. 2023) were selected for refinement using energy levels from MARVEL. For the $X\,^1\Sigma^+$ state,

[1]Freely available at github.com/exomol/Duo

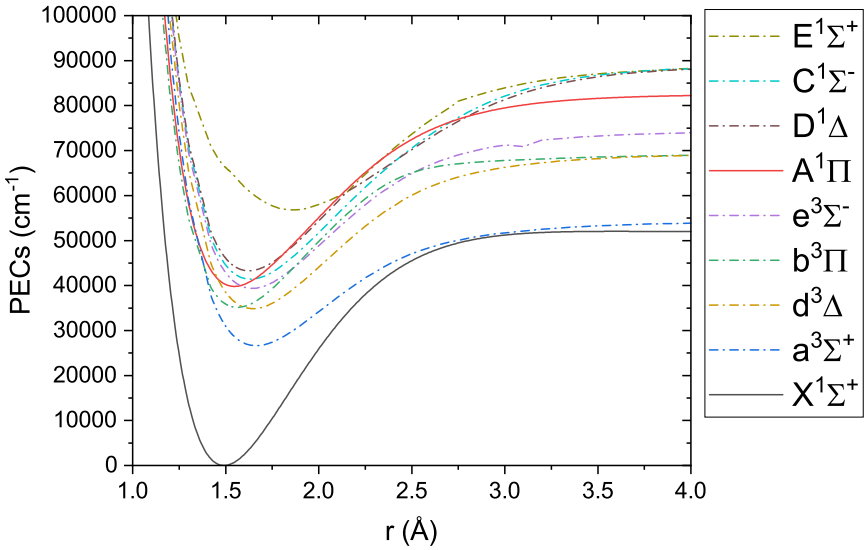

Figure 3. Empirical PECs of PN used as part of our new spectroscopic model (solid lines) and ab initio PECs of other electronic states of PN from our previous work (Semenov et al. 2021). Table 1 of the previous work also contains ab initio spectroscopic constants that could be helpful for the reader.

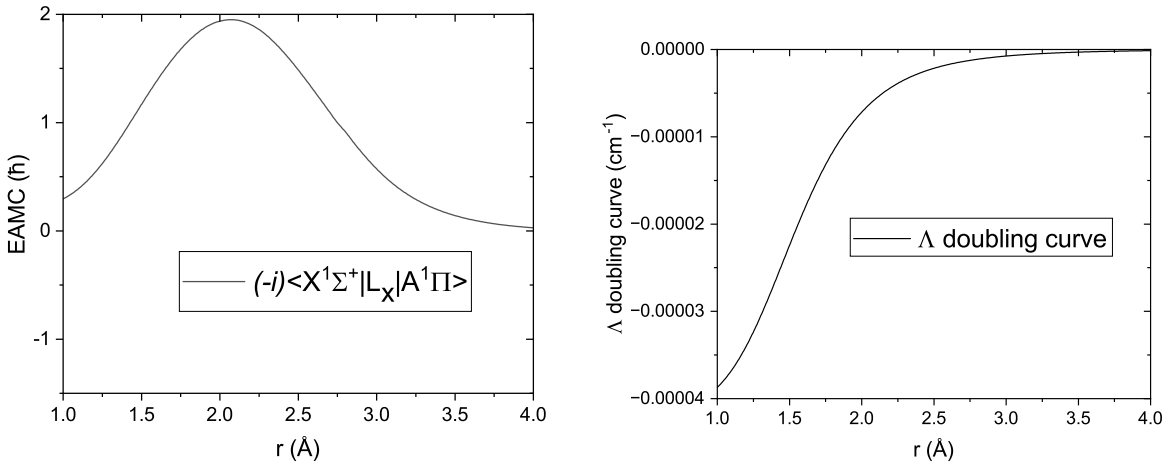

Figure 4. Fitted electronic angular momenta and Λ-doubling coupling curves of PN used in our spectroscopic model.

we used an empirical PEC of PN taken from Ushakov et al. (2023), where it was represented by the extended Hulburt–Hirschfelder potential as given by

$$V_{\rm EHH}(r) = D_{\rm e}\left[\left(1-e^{-q}\right)^2 + cq^3\left(1+\sum_{i=1}^{3} b_i q^i\right)e^{-2q}\right], \quad (1)$$

with $D_{\rm e}$ as a dissociation energy and $q = \alpha\,(r - r_{\rm e})$. $D_{\rm e}$ was kept at the value of 51 297 cm^{-1} calculated by Ushakov et al. (2023).

For the $A\,^1\Pi$ state, the initial PEC, calculated using internally contracted multireference configuration interaction with a Davidson correction (icMRCI + Q) with the aug-cc-pV5Z-DK basis set, was taken from our previous work (Semenov et al. 2021) and represented analytically by an extended Morse potential (Lee et al. 1999), which is described by

$$V(r) = V_{\rm e} + (A_{\rm e} - V_{\rm e})\left(1 - \exp\left[-\left(\sum_{i=0}^{N} a_i \xi_p(r)^i\right)(r - r_{\rm e})\right]\right)^2, \quad (2)$$

where $A_{\rm e}$ is the dissociation asymptote of $A\,^1\Pi$, $V_{\rm e}$ is the potential minimum, a_i are expansion coefficients, $r_{\rm e}$ is the equilibrium bond length of the electronic state, and $\xi_p(r)$ is a Šurkus variable (Šurkus, Rakauskas & Bolotin 1984) given by

$$\xi_p(r) = \frac{r^p - r_{\rm e}^p}{r^p + r_{\rm e}^p}. \quad (3)$$

The dissociation asymptote, $A_{\rm e}$, coming from the dissociation channel $P(^2D) + N(^2D)$ was set to 82 500 cm^{-1} as calculated from the atomic energies using the NIST atomic spectra data base (Kramida et al. 2020) rounded to 3 significant figures, while $V_{\rm e}$, $r_{\rm e}$, and a_i are treated as adjustable parameters.

3.2 Couplings

To construct a high accuracy model while also restricting the model to the two states for which we have extensive empirical data, we added two couplings. First, we included an electronic angular momentum coupling curve (EAMC) $\langle X\,^1\Sigma^+|L_x|A\,^1\Pi\rangle$, which we took from our previous work (Semenov et al. 2021). The ab initio EAMC was given

Table 3. RMSE (cm^{-1}) of the calculated energy term values of the $X\,^1\Sigma^+$ state as compared to the experimentally derived (MARVEL) values ($v = 0 \ldots 10$) for the rovibrational DUO values from the current model (PaiN) and the YYLT values (Yorke et al. 2014).

	RMSE	
v	PaiN	YYLT
0	0.0038	0.0029
1	0.0057	0.0053
2	0.0888	0.0994
3	0.0925	0.1257
4	0.1053	0.1703
5	0.1233	0.2266
6	0.1033	0.2196
7	0.0694	0.1358
8	0.0543	0.0802
9	0.0828	0.0934
10	0.0892	0.2938

Table 4. RMSE (cm^{-1}) of the calculated energy term values of the $A\,^1\Pi$ state from the current model as compared to the experimentally derived (MARVEL) values ($v = 0 \ldots 7, 9$).

v	RMSE
0	0.276
1	1.495
2	2.666
3	0.871
4	0.214
5	0.502
6	0.295
7	0.973
9	0.313

an analytical shape via the morphing functionality in DUO, by using a polynomial decay form given as

$$F(r) = \sum_{k=0}^{N} B_k z^k \left(1 - \xi_p\right) + \xi_p B_\infty, \tag{4}$$

with

$$z = (r - r_{\rm ref})\, e^{-\beta_2 (r - r_{\rm ref})^2 - \beta_4 (r - r_{\rm ref})^4}, \tag{5}$$

where $r_{\rm ref}$ is a reference coordinate for the expansion, in our case set to the minimum of the ground state potential, β_2 and β_4 are damping factors, B_k are expansion coefficients with B_∞ typically set to 1 and ξ is a Šurkus variable as in equation (3).

A Λ-doubling empirical curve was also included for the $A\,^1\Pi$ state, using the 'lambda-q' functionality in DUO. It was also given an analytical form of equation (4) with a single expansion term.

3.3 Refinement

We refined our spectroscopic model of PN represented by the PECs and coupling curves to the MARVEL energies. Overall, 12 parameters were fitted across 4 functions to 1224 energy levels from MARVEL with the angular momentum J ranging from 0 to 61. These parameters as part of the overall fit are given in the supplementary material as part of the final DUO input file used for the calculations. The fitted PECs and couplings can be seen in Figs 3 and 4. The PEC of the $X\,^1\Sigma^+$ from Yorke et al. (2014) was also refined because of the expanded range of available energy level data to fit to and to account for the electronic angular momenta coupling with the $A\,^1\Pi$ state.

The root mean square error (RMSE) of the overall fit is 0.971 cm^{-1}, where the RMSE of the $X\,^1\Sigma^+$ state and $A\,^1\Pi$ state energies are 0.26 and 1.24 cm^{-1}, respectively. In Table 3, we provide RMSEs of the calculated energy term values of the $X\,^1\Sigma^+$ state, comparing the current model and energies from the previous YYLT line list (Yorke et al. 2014). While there is a slight increase in the root mean square (RMS) for the $v = 0, 1$, it can be seen that the $v = 2 \ldots 10$ are better fitted within our model. It is worth noting that in the original paper by Yorke et al. (2014), the model was fitted to data based on 147 lines ($v \leq 4$) and effective vibrational term values ($v \leq 11$, $J = 0$), whereas in our current work we have expanded that to 2838 active lines as described in the MARVEL section of this paper with the overall more extended J and v coverage. We also provide an overview of the RMSE of the $A\,^1\Pi$ state of our model in Table 4. The majority of the residuals driving the RMS of the fit are the perturbed v states of $A\,^1\Pi$ as can be seen in Fig. 5 (see also the discussion of the perturbations of $A\,^1\Pi$ in Section 2.2). The sources of perturbations are believed to be dark electronic states, namely $e\,^3\Sigma^-$, $b\,^3\Pi$, $d\,^3\Delta$, $D\,^1\Delta$, and $C\,^1\Sigma^-$ (Ghosh et al. 1981; Le Floch et al. 1996), see Fig. 3 and also discussion in Section 2.2, and are especially strong around the predicted intersections listed in Table 2.

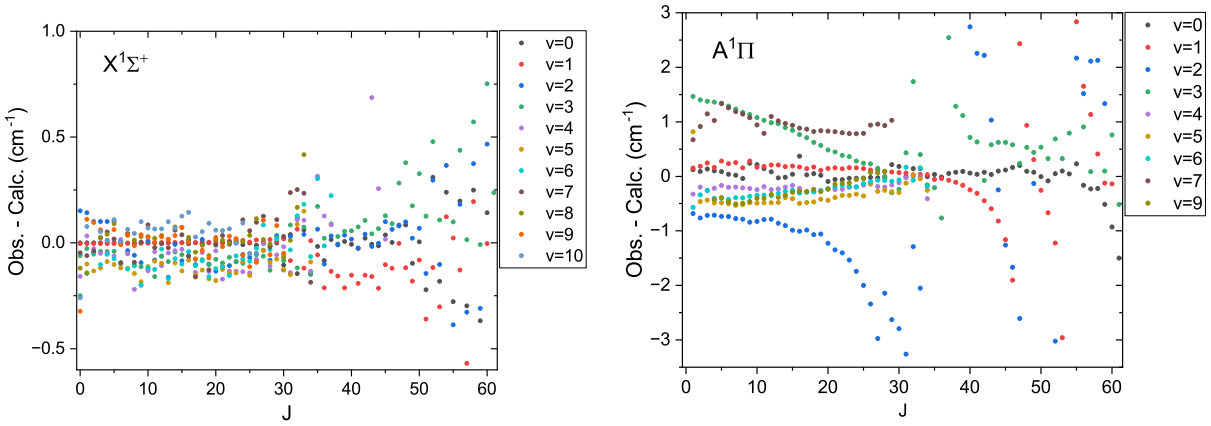

Figure 5. Visual representation of the MARVEL residuals (Obs.–Calc.) for the $A\,^1\Pi$ and $X\,^1\Sigma^+$ state levels.

Table 5. Line list statistics for each isotopologue of PN.

Isotopologue	g_{ns}	N_{states}	N_{trans}
$^{31}P^{14}N$	6	30327	1333445
$^{31}P^{15}N$	4	31563	1438181

Table 6. Description of the $A\,^1\Pi$ states, where the DUO energies have been selected to be replaced either with MARVEL or EH values in the MARVELization procedure.

v	Range of J's substituted
2	$J = 1 \cdots 29$
3	$J = 1 \cdots 29$
4	$J = 1 \cdots 28$
5	$J = 1 \cdots 26$
6	$J = 2 \cdots 20$
7	$J = 2 \cdots 28$
9	$J = 1 \cdots 24$

3.4 (Transition) dipole moment curves

The $X\,^1\Sigma^+$ state permanent DMC of Ushakov et al. (2023) was used. It was represented using the following functional form:

$$d_{\rm irreg}(r;n,k) = \frac{\left[1-\exp(-\alpha r)\right]^n}{\sqrt{\left(r^2-a_1^2\right)^2+b_1^2}\sqrt{\left(r^2-a_2^2\right)^2+b_2^2}} \sum_{i=0}^{k} c_i \left(1-2e^{-\beta r}\right)^i \quad (6)$$

as recommended by Medvedev & Ushakov (2022). By using this form, we aim to reduce the numerical noise in the intensities of high overtones as well as the associated saturation at high wavenumbers, leading to the so-called overtone plateaus (Medvedev et al. 2016).

For the transition dipole moment curve (TDMC) of the $A\,^1\Pi$–$X\,^1\Sigma^+$ system, we chose the ECP10MWB ab initio dipole calculated using icMRCI + Q from our previous work (Semenov et al. 2021), where it was shown to provide the closest lifetimes to the experiment. The ab initio TDMC was given on a grid and then scaled through the DUO 'morphing' by a factor of 1.28 to match the experimental lifetimes as described in Section 4.3.

4 LINE LIST AND SPECTRA

The PaiN line lists for two isotopologues of PN, $^{31}P^{14}N$ and $^{31}P^{15}N$, were produced with DUO using the empirically refined and ab initio curves as described above. For the main isotopologue $^{31}P^{14}N$, it contains 1333 445 transitions and 30 327 states for the $X\,^1\Sigma^+$ and $A\,^1\Pi$ states covering the wavenumber range up to 82 500 cm^{-1} (i.e. up to the dissociation of $A\,^1\Pi$), $v = 0 \ldots 63$ for $X\,^1\Sigma^+$ and $v = 0 \ldots 74$ and $J = 0 \ldots 210$. For $^{31}P^{15}N$, only the atomic mass of ^{15}N was changed in the DUO calculations. We simply do not have enough experimental data on minor isotopologues to verify the validity of any isotopologue extrapolation procedures, described in McKemmish et al. (2024). Further details on the number of states and transitions in each isotopologue are given in Table 5.

4.1 Energy levels

The DUO calculated energies were replaced with the MARVEL values (MARVELized), where available. We also used PGOPHER (Western 2017) to obtain EH energies to cover gaps in the MARVEL data of the $A\,^1\Pi$ state, using the constants provided by Ahmad & Hamilton (1995) and Ghosh et al. (1981). The PGOPHER file used is available as part of the supplementary material. In places where there were gaps in MARVEL energy levels in the range of $J = 0 \ldots 30$ for $A\,^1\Pi$ state, we ran an analysis to determine whether DUO or EH energies give better agreement with MARVEL within that range. Where EH

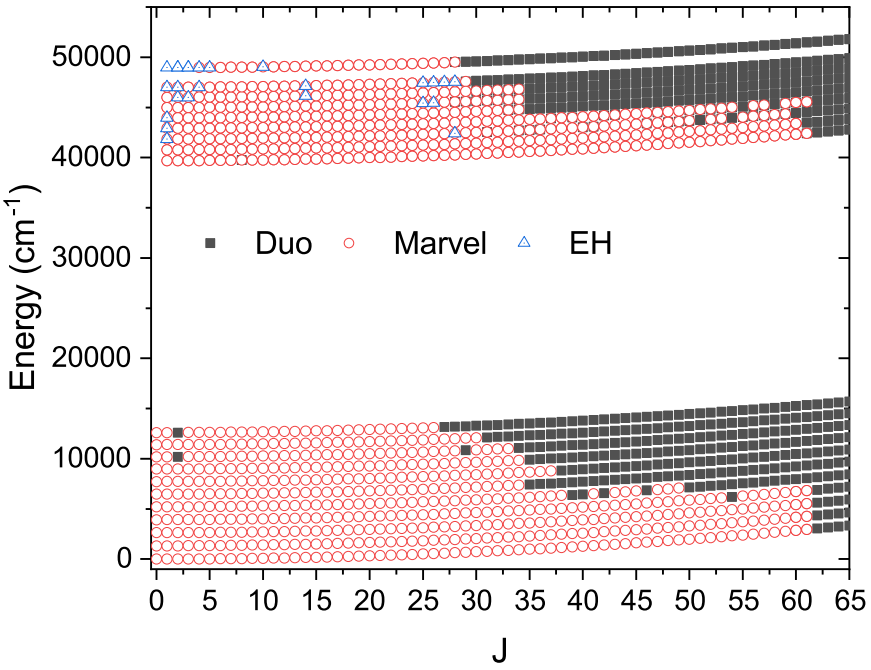

Figure 6. Visual representation of the sources of energy levels in the PaiN line list. DUO values, MARVEL values, and EH values for the vibrational states used in the MARVELization procedure. The states shown in the graph represent only those with experimental data available, namely $v = 0 \ldots 11$ for $X\,^1\Sigma^+$ and $v = 0 \ldots 7, 9$ for $A\,^1\Pi$.

Table 7. Constants ΔT, $\Delta\omega$, and ΔB (cm^{-1}) defining state-dependent uncertainties via equation (7) for 'Ca' and 'EH' energy levels.

State	ΔT	$\Delta\omega$	ΔB
$X\,^1\Sigma^+$	0.057	0.05	0.0001
$A\,^1\Pi$	0.237	0.05	0.0001

Table 8. Comparison of lifetimes from (A) our current work, (B) Semenov et al. (2021), and (C) Qin et al. (2019). An experimental lifetime 227 ± 70 ns was reported by Moeller et al. (1975) for $v' = 0$ of $A\,^1\Pi$, which is in good agreement with our results.

	$A\,^1\Pi$ /ns		
v'	A	B	C
0	222.9	341.3	659.4
1	227.2	334.6	674.3
2	231.9	338.9	660.8
3	236.6	344.3	646.5
4	241.4	349.8	642.2
5	246.3	356.2	643.0
6	251.3	361.6	632.1
7	256.4	368.1	610.6
8	261.5	376.3	607.4
9	266.6	392.4	598.6
10	271.6	399.3	583.8
11	276.8	407.3	581.8
12	281.9	413.0	566.8
13	287.1	420.7	565.3
14	292.2	431.3	553.1

energies were in better agreement with MARVEL energies, DUO energies were substituted with EH energies. The summary of ranges of DUO energies substituted by EH, where MARVEL energies were not available, is given in Table 6, with only 26 $A\,^1\Pi$ rovibronic energy levels substituted with EH energies overall.

We have used the labels 'Ca', 'EH', and 'Ma' in the penultimate column of the states file to indicate if the energy value is calculated using DUO, derived using EH (PGOPHER), or using MARVEL, respectively (McKemmish et al. 2024). It is worth noting that due to the perturbation of the $A\,^1\Pi$ rovibronic levels through near-lying dark states, we decided not to extrapolate MARVEL energy levels to higher values of J using the predicted shift methodology as suggested by McKemmish et al. (2024; as part of the QuadHybrid approach), as we could not guarantee the accuracy of extrapolated energy levels. A visual representation of the sources of energy levels is given in Fig. 6 for the vibronic states affected by the MARVELization.

The uncertainty values in the States file correspond to two cases: the MARVEL uncertainties are used for MARVELized energies, while for the DUO and EH calculated values, the following approximate expression is used:

$$\sigma(\text{ state }, J, v) = \Delta T + \Delta\omega v + \Delta B J(J+1), \tag{7}$$

where ΔT, $\Delta\omega$, and ΔB are electronic state dependent constant, given in Table 7. For the $X\,^1\Sigma^+$ and $A\,^1\Pi$ states, uncertainties were estimated based on the progression of residuals from Fig. 5 as average increases of obs.–calc. in v and J for each state shown. The uncertainties for the levels affected by the perturbations were increased according to the corresponding MRSEs.

4.2 Partition function

The partition function (PF) is an important tool when linking the energy levels of a molecule to its macroscopic properties, enabling predictions in astrophysical and atmospheric contexts. As such, as part of this work, we have computed PF for $^{31}P^{14}N$ and $^{31}P^{15}N$ as part of our semi-empirical line list. The function was computed using

$$Q(T) = \sum_i g_i^{\text{tot}}\, e^{-\frac{c_2 \tilde{E}_i}{T}}, \tag{8}$$

where c_2 is the second radiation constant, T is temperature in Kelvin, $\tilde{E}_i$ is the total rovibronic energy in cm^{-1} of a state i, and g_i^{tot} is the total state degeneracy given by

$$g_i^{\text{tot}} = g_{\text{ns}}(2J_i + 1), \tag{9}$$

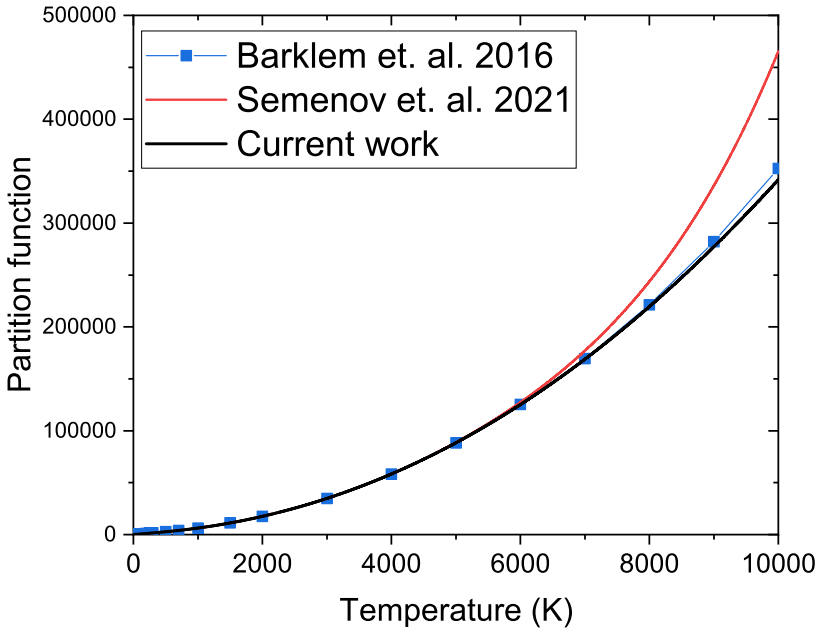

Figure 7. Comparison of PFs between current work, previous work Semenov et al. (2021) and that of Barklem & Collet (2016).

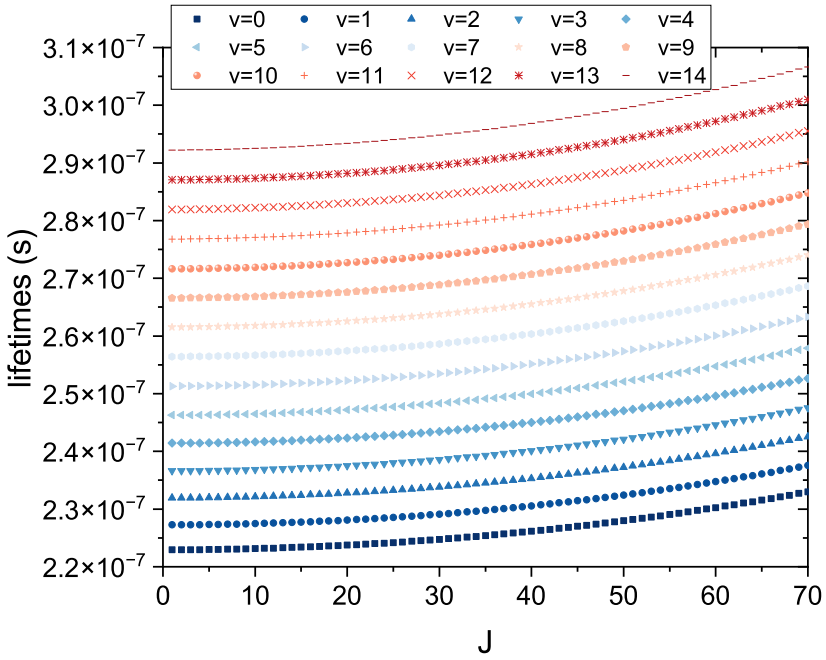

Figure 8. Lifetimes of the $A\,^1\Pi$ state.

Table 9. Extract from the PaiN .state file.

i	$\tilde{E}$ (cm^{-1})	g_i	J	Unc. (cm^{-1})	τ (s^{-1})	g	Parity		State	v	Λ	Σ	Ω	Label	$\tilde{E}$ (cm^{-1})
31	39690.318649	18	1	0.198704	2.2294E-07	0.500000	+	f	A1Pi	0	1	0	1	Ma	39690.342964
32	40778.595433	18	1	0.100000	2.2726E-07	0.500000	+	f	A1Pi	1	1	0	1	Ma	40778.599149
33	41852.997294	18	1	0.759055	2.3190E-07	0.500000	+	f	A1Pi	2	1	0	1	Ca	41852.997294
34	42912.839136	18	1	0.809055	2.3664E-07	0.500000	+	f	A1Pi	3	1	0	1	Ca	42912.839136
35	43957.866467	18	1	0.859055	2.4142E-07	0.500000	+	f	A1Pi	4	1	0	1	Ca	43957.866467
36	44989.841525	18	1	0.700000	2.4626E-07	0.500000	+	f	A1Pi	5	1	0	1	Ma	44988.062552
37	46002.911525	18	1	0.500000	2.5128E-07	0.500000	+	f	A1Pi	6	1	0	1	Ma	46003.572725
38	47004.651492	18	1	1.009055	2.5642E-07	0.500000	+	f	A1Pi	7	1	0	1	Ca	47004.651492
39	47991.618462	18	1	1.059055	2.6151E-07	0.500000	+	f	A1Pi	8	1	0	1	Ca	47991.618462

Notes. i: State counting number.
$\tilde{E}$: State energy term values in cm^{-1}, MARVEL, EH, or calculated (DUO).
g_i: Total statistical weight, equal to $g_{\rm ns}(2J+1)$.
J: Total angular momentum.
Unc.: Uncertainty, cm^{-1}.
τ: Lifetime (s^{-1}).
g: Landé g-factors.
$+/-$: Total parity.
State: Electronic state.
v: State vibrational quantum number.
Λ: Projection of the electronic angular momentum.
Σ: Projection of the electronic spin.
Ω: Projection of the total angular momentum, $\Omega = \Lambda + \Sigma$.
Label: 'Ma' is for MARVEL, 'EH' is for Effective Hamiltonian and 'Ca' is for Calculated.
$\tilde{E}$: State energy term values in cm^{-1}, calculated (DUO).

where $g_{\rm ns}$ is the nuclear weight spin-statistic. ExoMol uses the HITRAN convention, represented by the full nuclear statistical weight, meaning that for ^{31}P^{14}N $g_{\rm ns} = 6$ and for ^{31}P^{15}N $g_{\rm ns} = 4$, unlike the standard astrophysics convention, where $g_{\rm ns}$ is not included in PF.

Fig. 7 compares the PF between our current work, our previous ab initio work (Semenov et al. 2021) and that of Barklem & Collet (2016). We calculate our PF in a similar procedure used previously in Semenov et al. (2021) using a 1 K temperature step. For comparison of the ^{31}P^{14}N PF with Barklem & Collet (2016), we multiply their values by a factor of six to account for the lack of nuclear weight spin-statistic in their calculations, which we include. Our PF is in good agreement with previous results up to 5000 K but is then lower than the results of Semenov et al. (2021). The differences at higher temperatures can be explained by the additional electronic states included in the ab initio study (Semenov et al. 2021). We fix the maximum temperature of PaiN to be 5000 K.

Table 10. Extract from the .trans file of the PaiN line list for $^{31}P^{14}N$.

f	i	A_{fi} (s^{-1})	$\tilde{\nu}_{fi}$
77	6	1.0583E−10	13009.188326
78	6	1.2843E−11	14104.631827
79	6	3.0917E−12	15185.086622
80	6	1.4723E−12	16250.408774
81	6	3.0994E−13	17300.443346
82	6	1.2750E−14	18335.023853
83	6	1.7852E−14	19353.971649
84	6	2.2823E−14	20357.095245
85	6	1.3905E−14	21344.189551

Notes. f: Upper state counting number.
i: Lower state counting number.
A_{fi}: Einstein-A coefficient in s^{-1}.
$\tilde{\nu}_{fi}$: transition wavenumber in cm^{-1}.

4.3 Lifetimes

As part of the PaiN line list, we provide lifetimes for the $X\,^1\Sigma^+$ and $A\,^1\Pi$ states in our model. The lifetimes are calculated using EXOCROSS for each unique rovibronic energy level, utilizing the .states and .trans files. EXOCROSS uses the following equation to calculate lifetimes:

$$\tau_i = \frac{1}{\sum_{j<i} A_{ij}}, \tag{10}$$

where τ_i is radiative lifetime, A_{ij} is Einstein's A coefficients, and i and j stand for upper and lower states, respectively.

There is only one experimental measurement of the lifetime of $^{31}P^{14}N$ for the $A\,^1\Pi v = 0$ state, and it is equal to 227 ± 70 ns. We used this lifetime to scale our $A\,^1\Pi$–$X\,^1\Sigma^+$ transition dipole by a factor of 1.28 to get within reasonable accuracy. Table 8 provides a comparison of the lifetimes produced by our scaled dipole and previous works (Qin et al. 2019; Semenov et al. 2021). Fig. 8 shows the lifetimes for $J = 0 \ldots 70$ rotational states of the first 14 vibrational levels of $A\,^1\Pi$. From the figure, we can see that there is little to no J dependence in the $A\,^1\Pi$ lifetimes. It is also worth noting that because we only included two electronic states in our model, the lifetimes appear unperturbed which would not be the case should we include adjacent electronic states for $A\,^1\Pi$.

4.4 Line lists and opacities

The line list is provided in state and transition files, as is customary for the ExoMol format (Tennyson, Hill & Yurchenko 2013; Tennyson et al. 2024b). Extracts from the states and trans files are shown in Tables 9 and 10, respectively; the full files are available from www.exomol.com. The States file contains state IDs, energy term values (cm^{-1}), state uncertainties (cm^{-1}), Landé-g factors (Semenov, Yurchenko & Tennyson 2017), lifetimes (s) (Tennyson et al. 2016), and quantum numbers. The transition file contains the state IDs and Einstein A coefficients (s^{-1}). The PFs are also included in the standard line list compilation on a grid of 1 K between 0 and 10 000 K.

Temperature- and pressure-dependent molecular opacities of $^{31}P^{14}N$ based on the PaiN line list have been generated using the ExoMolOP procedure (Chubb et al. 2021) for four exoplanet atmospheric retrieval codes: ARCiS (Min et al. 2020), TauREx (Al-Refaie et al. 2021), NEMESIS (Irwin et al. 2008), and petitRADTRANS (Molliére et al. 2019). For the line broadening, we assumed an 86 per cent H_2 and 14 per cent He atmosphere and Voigt line profile.

An overview of the simulated spectra of the $A\,^1\Pi$–$X\,^1\Sigma^+$ and $X\,^1\Sigma^+$–$X\,^1\Sigma^+$ bands at different temperatures is given in Fig. 9. Owing to the specially constructed permanent $X\,^1\Sigma^+$ DMC (Ushakov et al. 2023) used, the intensities of the $X\,^1\Sigma^+$ overtone bands drop exponentially with no non-physical plateau-lie features.

4.5 The $A\,^1\Pi$–$X\,^1\Sigma^+$ band system

Originally discovered by Curry et al. (1933), the $A\,^1\Pi$–$X\,^1\Sigma^+$ band system has proved to be difficult to study due to the many perturbations from the near-lying electronic states as discussed in Section 2.2 and shown previously experimentally by Le Floch et al. (1996) and Ghosh et al. (1981). Below, we present simulated spectra of this band and compare them with observed results. Fig. 10 provides a comparison of the rovibronic absorption spectrum of the $A\,^1\Pi$–$X\,^1\Sigma^+$ (2,0) band between the simulated spectrum and observations reported by Le Floch et al. (1996). As can be seen, the simulated spectrum accurately reproduces the experimental observations even for the perturbed $v = 2$ state in $A\,^1\Pi$. There is a notable improvement of 2217 cm^{-1} shift in comparison to our previous work (Semenov et al. 2021), which is achieved by fitting the PEC to experimental data and using MARVELization. The absorption spectrum was simulated with a Gaussian profile of half-width at half-maximum (HWHM)

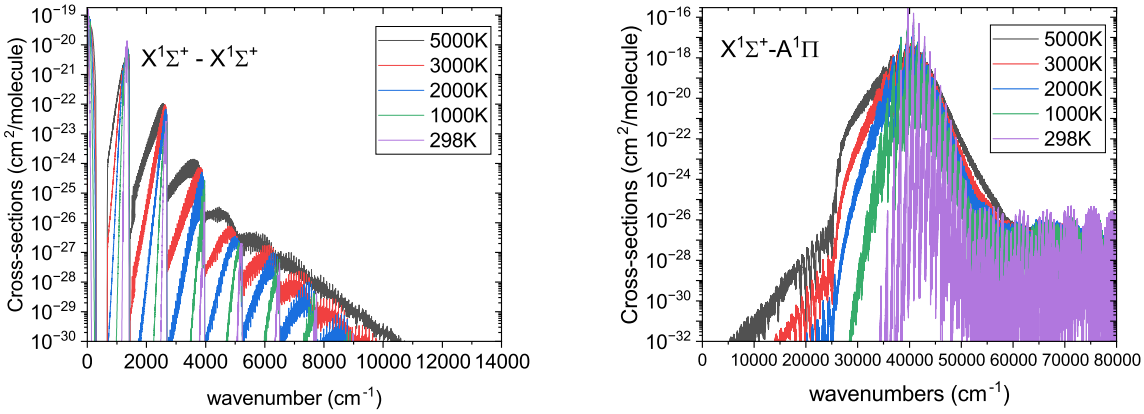

Figure 9. Overview of simulated $A\,^1\Pi$–$X\,^1\Sigma^+$ and $X\,^1\Sigma^+$–$X\,^1\Sigma^+$ absorption spectra, both calculated at different temperatures with a Gaussian profile of HWHM = 1 cm^{-1}.

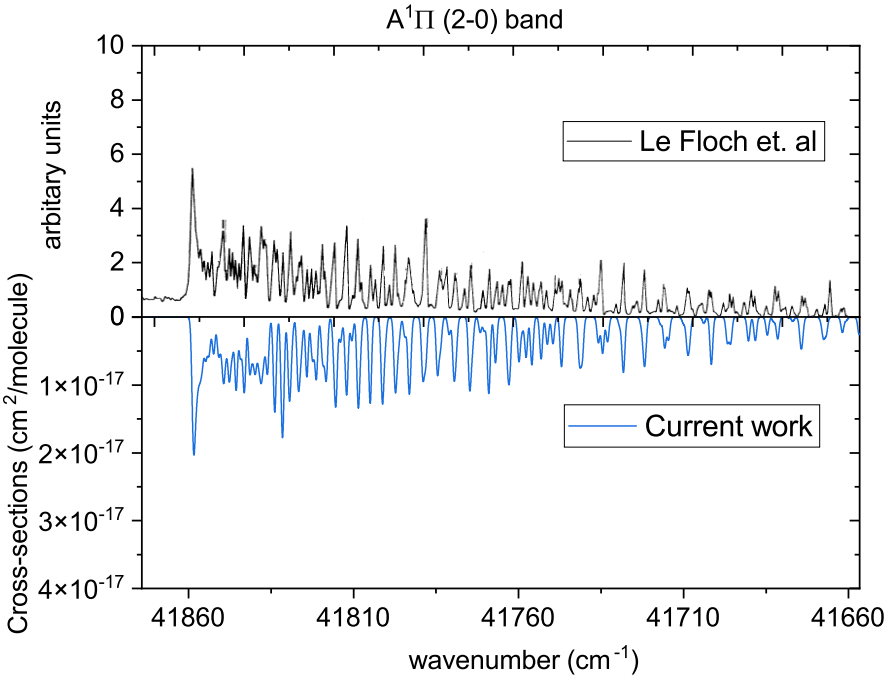

Figure 10. Comparison of the $A\,^1\Pi$–$X\,^1\Sigma^+$ (2,0) simulated absorption band (lower panel) with that recorded by Le Floch et al. (1996; upper panel). The spectrum was simulated at T =1173.15 K with a Gaussian profile of HWHM = 0.5 cm^{-1}.

= 0.5 cm^{-1} at a temperature of 1173.15 K which was extracted from the experimental work.

Fig. 11 offers an illustration of the $A\,^1\Pi$–$X\,^1\Sigma^+$ emission spectrum calculated using PaiN and compared to a non-LTE (non-local thermal equilibrium) emission spectrum reported by Moeller & Silvers (1973). As an attempt to describe the complex non-LTE environment of the experiment, a simple, two-temperature non-LTE model (Pannier & Laux 2019) was used as implemented in EXOCROSS (Yurchenko, Al-Refaie & Tennyson 2018), with $T_{\rm rot}$ = 300 K (rotational) and $T_{\rm vib}$ = 3500 K (vibrational) temperatures. The figure also highlights vibrational bands in both the experimental and simulated spectra. Some bands in the simulated spectra are still too weak to be seen, namely (0,2), (1,3), (0,3), and (3,1), and would require a more sophisticated non-LTE model for better agreement.

5 CONCLUSIONS

New line lists for ^{31}P^{14}N and ^{31}P^{15}N are presented, covering wavenumbers in the range from 0 to 82 500 cm^{-1}. The PaiN line lists supersede the original PN ExoMol line lists YYLT (Yorke et al. 2014) by extending it to the $A\,^1\Pi$–$X\,^1\Sigma^+$ band. PaiN is available from www.exomol.com.

As part of the line list update, an MARVEL analysis for ^{31}P^{14}N was performed using 6005 measured rovibronic transitions. All experimental line positions from the literature (to the best of our knowledge) covering the infrared (IR) and UV regions of $X\,^1\Sigma^+$–$X\,^1\Sigma^+$ and $A\,^1\Pi$–$X\,^1\Sigma^+$ systems were collected and processed to generate a comprehensive, self-contained set of empirical energies of ^{31}P^{14}N. An accurate spectroscopic model for PN in $X\,^1\Sigma^+$ and $A\,^1\Pi$ was built using previously calculated ab initio TDMCs and empirically refined PECs, EAMC, and a Λ-doubling curve.

The line list for ^{31}P^{14}N was MARVELized, where the DUO calculated energies were replaced with the MARVEL or EH values (where

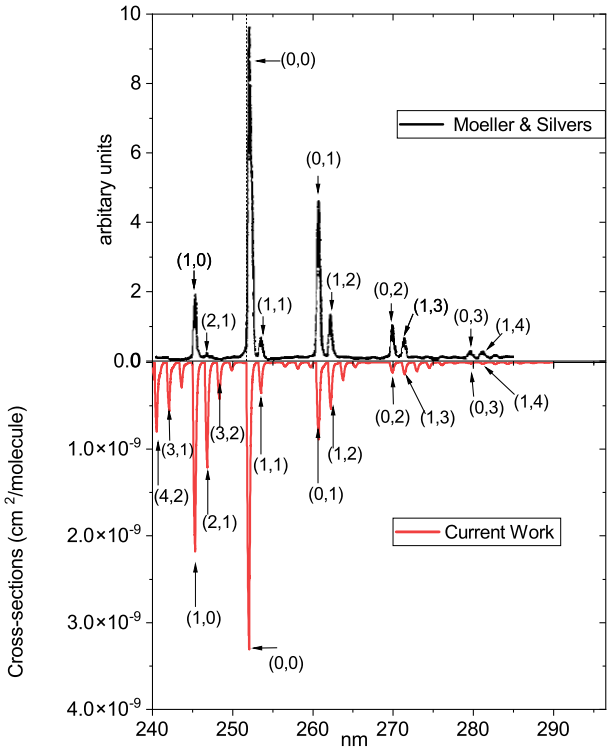

Figure 11. Comparison of an $A\,^1\Pi$–$X\,^1\Sigma^+$ simulated emission spectrum (lower panel) with that recorded by Moeller & Silvers (1973; upper panel). The numbers in brackets represent the vibrational bands. The spectrum was simulated at $T_{\rm rot}$ = 300 K (rotational) and $T_{\rm vib}$ = 3500 K (vibrational) temperatures with a Gaussian profile of HWHM = 100 cm^{-1}.

available and applicable). The PaiN line list provides uncertainties of the rovibronic states in order to help in high-resolution applications. Comparisons of simulated spectra show close agreement with the experiment. By scaling the $A\,^1\Pi$–$X\,^1\Sigma^+$ TDMC an agreement between computed reported lifetimes has been achieved.

The new line lists should help detect PN in the UV region and be useful in atmospheric chemistry applications, particularly atmospheric chemistry modelling. Further improvements to the line lists can include adding the dark states to the model to accurately model the $A\,^1\Pi$ perturbations and the expansion of the line list to include the $E\,^1\Sigma^+$ state. Both of these improvements will require further ab initio calculations coupled with additional experimental data not currently available.

ACKNOWLEDGEMENTS

This work was supported by the European Research Council (ERC) under the European Union's Horizon 2020 research and innovation programme through advance grant number 883830 and STFC project no. ST/Y001508/1. NE-K's work is supported by ASPIRE AARE grant number AARE20-000329-00001 and Khalifa University of Science and Technology grant 8474000336-KU-SPSC.

DATA AVAILABILITY

The data underlying this article are available in the article and in its online supplementary material. The line list and associated data (PFs, opacities, temperature-dependent absorption cross-sections) for PN are available from www.exomol.com. The codes used in this work, namely DUO and EXOCROSS, are freely available via https://github.com/exomol.

REFERENCES

Abbiche K., Salah M., Marakchi K., Kabbaj O. K., Komiha N., 2014, Mol. Phys., 112, 117
Ahmad I. K., Hamilton P. A., 1995, J. Mol. Spectrosc., 169, 286
Al-Refaie A. F., Changeat Q., Waldmann I. P., Tinetti G., 2021, ApJ, 917, 37,
Barklem P. S., Collet R., 2016, A&A, 588, A96
Bowesman C. A., Akbari H., Hopkins S., Yurchenko S. N., Tennyson J., 2022, J. Quant. Spectrosc. Radiat. Transf., 289, 108295
Cazzoli G., Cludi L., Puzzarini C., 2006, J. Mol. Struct., 780, 260
Chubb K. L. et al., 2024, RASTI, 3, 636,
Chubb K. L. et al., 2021, A&A, 646, A21
Coquart B., Prudhomme J. C., 1981, J. Mol. Spectrosc., 87, 75
Curry J., Herzberg L., Herzberg G., 1933, J. Chem. Phys., 1, 749
De Beck E., Kami'nski T., Patel N. A., Young K. H., Gottlieb C. A., Menten K. M., Decin L., 2013, A&A, 558, A132
Eckhardt A. K., Riu M.-L. Y., Ye M., Muller P., Bistoni G., Cummins C. C., 2022, Nat. Chem., 14, 928
Fontani F., 2024, Frontiers Astron. Space Sci., 11, 1
Fontani F., Rivilla V. M., Caselli P., Vasyunin A., Palau A., 2016, ApJ, 822, L30
Fontani F., Rivilla V. M., van der Tak F. F. S., Mininni C., Beltran M. T., Caselli P., 2019, MNRAS, 489, 4530
Furtenbacher T., Császár A. G., 2012a, J. Quant. Spectrosc. Radiat. Transf., 113, 929
Furtenbacher T., Császár A. G., 2012b, J. Mol. Struct., 1009, 123
Furtenbacher T., Császár A. G., Tennyson J., 2007, J. Mol. Spectrosc., 245, 115
Ghosh S. N., Verma R. D., VanderLinde J., 1981, Can. J. Phys., 59, 1640
Gomes A. C. R., Souza A. C., Jasper A. W., Galvao B. R. L., 2023, Publ. Astron. Soc. Aust., 40, e011
Haasler D. et al., 2022, A&A, 659, A158
Hoeft J., Tiemann E., Törring T., 1972, Z. Naturforsch. A, A, 27, 703
Irwin P. G. J. et al., 2008, J. Quant. Spectrosc. Radiat. Transf., 109, 1136
Koelemay L. A., Gold K. R., Ziurys L. M., 2023, Nature, 623, 292
Kramida A., Ralchenko Y., Reader J., NIST ASD Team, 2020, Atoms, 8, 56
Le Floch A. C., Melen F., Dubois I., Bredohl H., 1996, J. Mol. Spectrosc., 176, 75
Lee E. G., Seto J. Y., Hirao T., Bernath P. F., Le Roy R. J., 1999, J. Mol. Spectrosc., 194, 197
Lefloch B. et al., 2016, MNRAS, 462, 3937
Liu H., Zhang H., Shi D., Zhu Z., 2022, Mol. Phys., 120, e2124202
Maki A. G., Lovas F. J., 1981, J. Mol. Spectrosc., 85, 368
McKemmish L. K., Bowesman C. A., Kefala K., Perri A. N., Syme A. M., Yurchenko S. N., Tennyson J., 2024, RASTI, 3, 565
Medvedev E. S., Ushakov V. G., 2022, J. Quant. Spectrosc. Radiat. Transfer, 288, 108255
Medvedev E. S., Meshkov V. V., Stolyarov A. V., Ushakov V. G., Gordon I. E., 2016, J. Mol. Spectrosc., 330, 36
Milam S. N., Halfen D. T., Tenenbaum E. D., Apponi A. J., Woolf N. J., Ziurys L. M., 2008, ApJ, 684, 618
Millar T. J., Bennett A., Herbst E., 1987, MNRAS, 229, 41P
Min M., Ormel C. W., Chubb K., Helling C., Kawashima Y., 2020, A&A, 642, A28
Moeller M. B., Silvers S. J., 1973, Chem. Phys. Lett., 19, 78
Moeller M. B., McKeever M. R., Silvers S. J., 1975, Chem. Phys. Lett., 31, 398
Molliére P., Wardenier J. P., van Boekel R., Henning T., Molaverdikhani K., Snellen I. A. G., 2019, A&A, 627, A67
Pannier E., Laux C. O., 2019, J. Quant. Spectrosc. Radiat. Transf., 222–223, 12
Qin Z., Zhao J. M., Liu L. H., 2019, J. Quant. Spectrosc. Radiat. Transf., 227, 47
Rivilla V. M. et al., 2018, MNRAS, 475, L30
Rivilla V. M. et al., 2020, MNRAS, 492, 1180
Semenov M., Yurchenko S. N., Tennyson J., 2017, J. Mol. Spectrosc., 330, 57
Semenov M., El-Kork N., Yurchenko S. N., Tennyson J., 2021, Phys. Chem. Chem. Phys., 23, 22057
Sil M. et al., 2021, AJ, 162, 119
Šurkus A. A., Rakauskas R. J., Bolotin A. B., 1984, Chem. Phys. Lett., 105, 291
Tennyson J., Hill C., Yurchenko S. N., 2013, in 6th International Conference on Atomic and Molecular Data and Their Applications ICAMDATA-2012. AIP, New York, p. 186
Tennyson J., Hulme K., Naim O. K., Yurchenko S. N., 2016, J. Phys. B-At. Mol. Opt. Phys., 49, 044002
Tennyson J., Furtenbacher T., Yurchenko S. N., Császár A. G., 2024a, J. Quant. Spectrosc. Radiat. Transf., 316, 108902
Tennyson J. et al., 2024b, J. Quant. Spectrosc. Radiat. Transf., 326, 109083
Thorne L. R., Anicich V. G., Prasad S. S., Huntress W. T., Jr, 1984, ApJ, 280, 139
Tian H., Fan Z., Wang Z., Fan Q., Ye Z., Gou F., Wei J., 2024, Spectroc. Acta Pt. A-Molec. Biomolec. Spectr., 304, 123381
Tóbiás R., Furtenbacher T., Tennyson J., Császár A. G., 2019, Phys. Chem. Chem. Phys., 21, 3473
Tobola R., Klos J., Lique F., Chalasinski G., Alexander M. H., 2007, A&A, 468, 1123
Tofan D., Velian A., 2020, ACS Central Sci., 6, 1485
Turner B. E., Bally J., 1987, ApJ, 321, L75
Ushakov V. G., Semenov M., Yurchenko S. N., Ermilov A. Y., Medvedev E. S., 2023, J. Mol. Spectrosc., 395, 111804
Verma R. D., Ghosh S. N., 1984, J. Phys. B-At. Mol. Opt. Phys., 17, 3529
Verma R. D., Ghosh S. N., Iqbal Z., 1987, J. Phys. B-At. Mol. Opt. Phys., 20, 3961
Western C. M., 2017, J. Quant. Spectrosc. Radiat. Transf., 186, 221
Wyse F. C., Gordy W., Manson E. L., 1972, J. Chem. Phys., 57, 1106
Yamaguchi T. et al., 2011, PASJ, 63, L37
Yorke L., Yurchenko S. N., Lodi L., Tennyson J., 2014, MNRAS, 445, 1383

Yurchenko S. N., Lodi L., Tennyson J., Stolyarov A. V., 2016, Comput. Phys. Commun., 202, 262
Yurchenko S. N., Al-Refaie A. F., Tennyson J., 2018, A&A, 614, A131
Zhu B. et al., 2024, ApJ, 964, 182
Ziurys L. M., Milam S. N., Apponi A. J., Woolf N. J., 2007, Nature, 447, 1094
Ziurys L. M., Schmidt D. R., Bernal J. J., 2018, ApJ, 856, 169

SUPPORTING INFORMATION

The following is provided as supporting information (1) the DUO input file that contains all the PN potential energy, dipole moment, and coupling curves used in this work; (2) the MARVEL input (transitions and segment) file and output (energy) file; (3) PGOPHER file with the EH constants used in this work; and (4) documented transitions by Verma et al. (1987).

Supplementary data are available at *MNRAS* online.

Please note: Oxford University Press is not responsible for the content or functionality of any supporting materials supplied by the authors. Any queries (other than missing material) should be directed to the corresponding author for the article.

This paper has been typeset from a TEX/LATEX file prepared by the author.